Available online at www.sciencedirect.com
ScienceDirect
Journal of Photochemistry and Photobiology A: Chemistry 183 (2006) 176–181
Journal of Photochemistry and Photobiology A:Chemistry
www.elsevier.com/locate/jphotochem

Influences of A- and B-site cations on the physicochemical properties of perovskite-structured $A(In_{1/3}Nb_{1/3}B_{1/3})O_3$ (A = Sr, Ba; B = Sn, Pb) photocatalysts

Su Gil Hur, Tae Woo Kim, Seong-Ju Hwang *, Jin-Ho Choy *

Center for Intelligent Nano-Bio Materials (CINBM), Division of Nano Sciences and Department of Chemistry, Ewha Womans University, Seoul 120-750, South Korea

Received 22 October 2005; received in revised form 27 February 2006; accepted 11 March 2006
Available online 17 March 2006

Abstract

We have investigated the effects of A- and B-site cation substitution on the physicochemical properties of perovskite-structured $A(In_{1/3}Nb_{1/3}B_{1/3})O_3$ (A = Sr, Ba; B = Sn, Pb) photocatalysts. X-ray diffraction, X-ray absorption and diffuse UV–vis spectroscopic analyses reveal that tetravalent Pb^{IV} or Sn^{IV} ions can be successfully incorporated into the octahedral B-site of the perovskite lattice, leading to a narrowing of bandgap energy (E_g). The substitution of such electronegative cations gives rise to the enhancement of photocatalytic activity to effectively decompose organic molecules. Interestingly, alkaline earth metal ions in the dodecahedral A-site with ionic bonding environment also affect significantly the band structure and photoefficiency of the perovskite compounds; a larger cation is beneficial for creating visible light driven photocatalytic activity through a decrease of E_g. This observation could be understood in terms of the weakening of transition metal–oxygen bond upon the expansion of unit cell. The present relationship between the chemical bonding nature of substituent cation and the band structure provides an efficient tool for designing and developing new efficient visible light active photocatalysts.

Keywords: Visible light active photocatalyst; Bandgap engineering; Cation substitution; Perovskite; Chemical bonding nature

1. Introduction

Over the past decades, semiconductive inorganic solids have attracted intense research interest due to their photocatalytic activity for the degradation of organic pollutants and/or the decomposition of water molecules [1,2]. Such a photodissociation driven by a semiconductor originates from a redox reaction with transient electrons or holes generated by an electronic transition from valence band (VB) to conduction band (CB). The efficiency of photocatalysts depends strongly on their band structures such as bandgap energy (E_g), the positions of VB and CB, etc. In this regard, there have been many attempts to optimize the band structure of the semiconductive photocatalyst such as dye sensitization, a coupling of different semiconductors, and so on [3–5]. Recently attempts have been made to modify the bandgap energy simply by substituting metal or oxygen ions in part in oxide lattice [6,7]. In particular, a perovskite-structured ABO_3 metal oxide can be a promising matrix for the chemical substitution, since it is stable enough to form a solid solution with diverse metal ions. In fact, there have been some reports about the substitution of transition metal ions into UV-active photocatalysts, leading to the decrease of E_g [8,9]. More recently we have shown that visible light driven photocatalytic activity can be induced by the incorporation of electronegative cations into an octahedral B-site of perovskite lattice [10]. On the other hand, there have been limited number of literatures about the influence of cation in a dodecahedral A-site on the bonding nature of photocatalysts [8a,11], since a covalent bond between B-site cation and oxygen is believed to be a main factor in determining the electronic structure of metal oxide photocatalyst near Fermi energy, rather than an ionic bond between A-site cation and oxygen.

In this study, we have investigated the influence of A-site cations as well as the B-site ones on the physicochemical properties of perovskite-structured $A(In_{1/3}Nb_{1/3}B_{1/3})O_3$ (A = Sr, Ba; B = Sn, Pb) photocatalysts and their chemical bonding nature

* Corresponding authors. Tel.: +82 2 3277 4370; fax: +82 2 3277 3419.
E-mail address: hwangsju@ewha.ac.kr (S.-J. Hwang).

1010-6030/$ – see front matter © 2006 Elsevier B.V. All rights reserved.
doi:10.1016/j.jphotochem.2006.03.014

and band structure have been systematically studied using X-ray diffraction (XRD), X-ray absorption (XAS) and diffuse UV–vis spectroscopy. In addition, the evolution of photocatalytic activities upon cation substitution has been studied by examining the decomposition of organic pollutants under UV–vis or visible light irradiation. On the basis of chemical bonding character, the effects of cation substitution on the A- and B-sites on the photoefficiency have been explained in terms of the evolution of metal–oxygen bonds.

2. Experimental

2.1. Sample preparation and characterization

Polycrystalline $A(In_{1/2}Nb_{1/2})O_3$ and $A(In_{1/3}Nb_{1/3}B_{1/3})O_3$ (A = Sr, Ba; B = Sn, Pb) samples were prepared by conventional solid-state reaction with the stoichiometric mixture of $SrCO_3$, $BaCO_3$, PbO_2, SnO_2, In_2O_3 and Nb_2O_3 at 950–1050 °C for several days in oxygen atmosphere. The crystal and band structures of the obtained perovskite-type compounds have been determined by XRD and diffuse UV–vis spectroscopy, respectively. Diffuse reflectance UV–vis spectra were obtained on a Perkin-Elmer Lambda 35 spectrometer equipped with an integrating sphere using $BaSO_4$ as a reference. The recorded reflectance data were used to estimate the bandgap energy by converting the reflectance data to the absorption ones through the Kubelka–Munk function [12]. The morphology and particle size for all the samples were determined by field emission-scanning electron microscopy (FE-SEM) using a JEOL JSM-6700F microscope. During FE-SEM experiments, semiquantitative energy dispersive spectroscopic (EDS) analysis was also carried out for several crystallites to confirm the incorporation of Sn or Pb ions into the perovskite lattice. XAS experiments were performed at Pb L_{III}-edge with the extended X-ray absorption fine structure (EXAFS) facility installed at the beam line 7C at the Pohang Light Sources (PLS) in Korea. XAS data were collected at room temperature in a transmission mode using gas-ionization detectors. All the present spectra were calibrated carefully by measuring the spectrum of Pb metal simultaneously. Data analysis for the experimental spectra was performed with standard procedure reported previously [13].

2.2. Measurement of photocatalytic activity

The photocatalytic reactions were carried out in a Pyrex reactor (30 mL) with quartz window, which was subjected to UV–vis or visible radiation. A 300-W Xe arc lamp (Muller) was used as a light source. Light passed through a 10-cm IR water filter and a UV cutoff filter ($\lambda > 300$ nm for UV illumination and $\lambda > 420$ nm for visible illumination), then the filtered light was focused onto the reactor. Methylene Blue (MB) and 4-chlorophenol (4-CP) were used as test substrates and their photocatalytic degradation in aqueous catalyst suspensions was examined as a function of the irradiation time. The concentration changes of MB and 4-CP were monitored spectrophotometrically by measuring the absorbance at $\lambda = 665$ and 485 nm, respectively, with an UV–vis spectrophotometer.

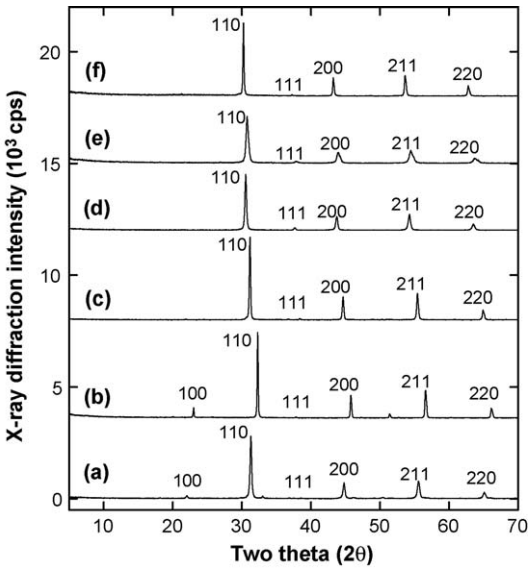

Fig. 1. Powder XRD patterns for: (a) $Sr(In_{1/2}Nb_{1/2})O_3$, (b) $Sr(In_{1/3}Nb_{1/3}Sn_{1/3})O_3$, (c) $Sr(In_{1/3}Nb_{1/3}Pb_{1/3})O_3$, (d) $Ba(In_{1/2}Nb_{1/2})O_3$, (e) $Ba(In_{1/3}Nb_{1/3}Sn_{1/3})O_3$ and (f) $Ba(In_{1/3}Nb_{1/3}Pb_{1/3})O_3$.

3. Results and discussion

3.1. Powder XRD and FE-SEM analysis

Fig. 1 represents the powder XRD patterns of the quaternary metal oxides $A(In_{1/3}Nb_{1/3}B_{1/3})O_3$ (A = Sr, Ba; B = Sn, Pb), together with those of the ternary $A(In_{1/2}Nb_{1/2})O_3$ compounds. All the diffraction peaks could be well indexed on the basis of perovskite structure with the cubic symmetry [8]. As listed in Table 1, the Ba-based compounds show a larger lattice parameter *a* than the corresponding Sr-based ones, since the Ba^{II} ion is bigger than the Sr^{II} ion [14]. Taking into account the fact that the

Table 1
Lattice parameters, unit cell volumes, tolerance factors and bandgap energies of $A(In_{1/2}Nb_{1/2})O_3$ and $A(In_{1/3}Nb_{1/3}B_{1/3})O_3$ with A = Sr, Ba and B = Sn, Pb

Sample	*a* (Å)	Unit cell volume (Å^3)	Tolerance factor	Bandgap energy (eV)
$Sr(In_{1/2}Nb_{1/2})O_3$	4.0595	66.899	0.95	3.62
$Sr(In_{1/3}Nb_{1/3}Sn_{1/3})O_3$	4.0533	66.593	0.95	3.48
$Sr(In_{1/3}Nb_{1/3}Pb_{1/3})O_3$	4.0617	67.008	0.94	3.10
$Ba(In_{1/2}Nb_{1/2})O_3$	4.1452	71.226	1.00	3.30
$Ba(In_{1/3}Nb_{1/3}Sn_{1/3})O_3$	4.1377	70.840	1.01	3.00
$Ba(In_{1/3}Nb_{1/3}Pb_{1/3})O_3$	4.1856	73.329	1.00	1.48

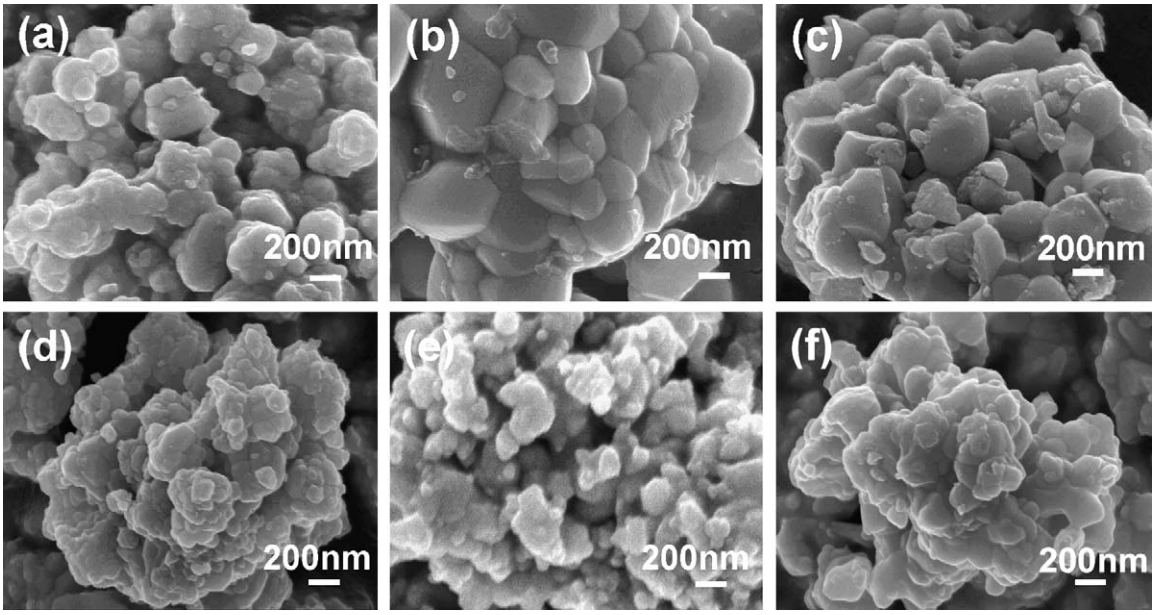

Fig. 2. FE-SEM images of: (a) $Sr(In_{1/2}Nb_{1/2})O_3$, (b) $Sr(In_{1/3}Nb_{1/3}Sn_{1/3})O_3$, (c) $Sr(In_{1/3}Nb_{1/3}Pb_{1/3})O_3$, (d) $Ba(In_{1/2}Nb_{1/2})O_3$, (e) $Ba(In_{1/3}Nb_{1/3}Sn_{1/3})O_3$ and (f) $Ba(In_{1/3}Nb_{1/3}Pb_{1/3})O_3$.

lattice parameter corresponds to the doubled distance of B–O bond in a cubic ABO_3 perovskite, the larger lattice parameter of the Ba-based compounds implies the elongation of metal (in B-site)–oxygen bond, compared to the Sr-based ones. The changes of crystallite morphology upon cation substitution were examined using FE-SEM measurements. As shown in Fig. 2, all of the present compounds display polygon-shaped crystallites with the average size of 0.1–0.3 μm. During the FE-SEM measurements, we have also carried out the EDS analysis, clearly demonstrating the partial replacement of In/Nb ions by Pb or Sn ion.

3.2. XANES spectroscopic analysis

The oxidation state of the substituted Pb ion was determined using XANES spectroscopy at Pb L_{III}-edge. Fig. 3 represents the Pb L_{III}-edge XANES spectra of $A(In_{1/3}Nb_{1/3}Pb_{1/3})O_3$ and the references PbO and PbO_2. The selection rule for photoelectric excitation in the dipolar approximation predicts that a transition to final states with orbital angular momentum quantum number l_f, which is different from initial state with l_i by ± 1 unit, is allowed [15]. Due to the presence of holes in the Pb 6s and 6d orbitals of $Pb^{IV}O_2$, this reference shows the pre-edge peak P corresponding to $2p_{3/2} \rightarrow 6s$ one as well as the main-edge peaks A and B corresponding to $2p_{3/2} \rightarrow 6dt_{2g}$ and $2p_{3/2} \rightarrow 6de_g$ transitions, respectively [16]. In contrast, an intense pre-edge peak P is absent in the reference spectrum of divalent $Pb^{II}O$ with a Pb electronic configuration of $[Xe]4f^{14}5d^{10}6s^2$. As shown in Fig. 3, both the perovskites exhibit a distinct pre-edge peak P, evidencing the tetravalent oxidation state of Pb in these compounds. This observation is cross-confirmed by the similar edge positions of $A(In_{1/3}Nb_{1/3}Pb_{1/3})O_3$ and the reference $Pb^{IV}O_2$, which are higher than that of the reference $Pb^{II}O$. As in the case of Pb-substituted compound, we have also confirmed that the tetravalent Sn^{IV} ions can be effectively stabilized in the perovskite lattice of $A(In_{1/3}Nb_{1/3}Sn_{1/3})O_3$ through the heat-treatment under $P_{O_2} = 1$ atm [10]. Since the electronegativity of an element is strongly dependent on its oxidation state [17], it is very important to stabilize the tetravalent oxidation states of lead or tin ion in realizing the present bandgap engineering strategy based on the electronegativity of metal cations.

3.3. Diffuse UV–vis spectroscopic analysis

The UV–vis spectra for the $A(In_{1/3}Nb_{1/3}B_{1/3})O_3$ compounds are illustrated in Fig. 4, together with those for $A(In_{1/2}Nb_{1/2})O_3$.

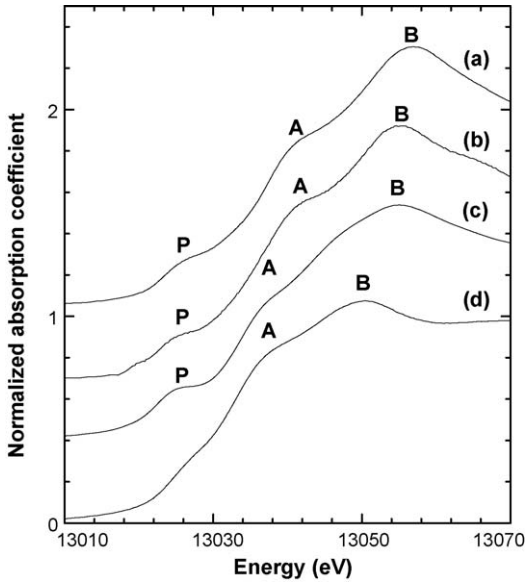

Fig. 3. Pb L_{III}-edge XANES spectra for: (a) $Sr(In_{1/3}Nb_{1/3}Pb_{1/3})O_3$, (b) $Ba(In_{1/3}Nb_{1/3}Pb_{1/3})O_3$, in comparison with the reference spectra for (c) PbO_2 and (d) PbO.

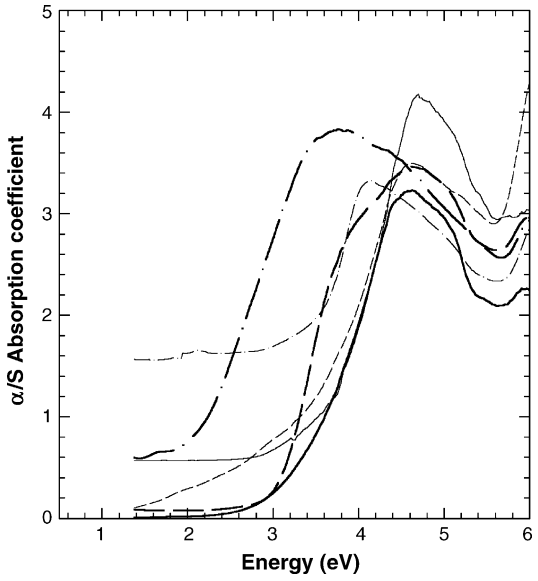

Fig. 4. Diffuse UV–vis spectra for $Sr(In_{1/2}Nb_{1/2})O_3$ (thin solid lines), $Sr(In_{1/3}Nb_{1/3}Sn_{1/3})O_3$ (thin dashed lines), $Sr(In_{1/3}Nb_{1/3}Pb_{1/3})O_3$ (thin dotted–dashed lines), $Ba(In_{1/2}Nb_{1/2})O_3$ (thick solid lines), $Ba(In_{1/3}Nb_{1/3}Sn_{1/3})O_3$ (thick dashed lines) and $Ba(In_{1/3}Nb_{1/3}Pb_{1/3})O_3$ (thick dotted–dashed lines).

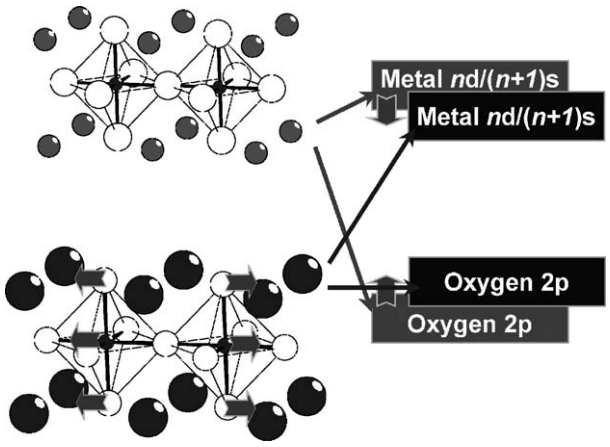

Fig. 5. A schematic model for the effect of A-site cation on the crystal and band structures of perovskite-structured photocatalysts.

Their E_g's were evaluated by a linear interpolation of α/S absorption coefficients [12]. As can be seen clearly from Fig. 4, a notable residual absorption is observable below bandgap energy for several compounds, especially for $Sr(In_{1/3}Nb_{1/3}Pb_{1/3})O_3$. This finding suggests that these compounds possess considerable number of oxygen vacancies leading to the formation of impurity states in the middle of bandgap. While the ternary metal oxide $Sr(In_{1/2}Nb_{1/2})O_3$ is an UV-active semiconductor with a wide bandgap separation of 3.6 eV, the incorporation of Pb or Sn ions gives rise to a distinct depression of the E_g value to 3.1 eV for Pb and 3.5 eV for Sn. Similar trend in the variation of bandgap energy upon B-site cation substitution was also observed for the Ba-based compounds (Table 1). This finding provides clear evidence that the bandgap energy of semiconductive ABO_3 perovskite can be manipulated simply by substituting the octahedral cation. Such a modification of band structure can be explained by an increase of covalent character of (B–O) bond upon electronegative metal substituent with high oxidation state. It has been well-known that the band structure of metal oxide semiconductor consists of metal nd/($n+1$)s and O 2p levels, which form the CB and VB, respectively [8]. In the case of the pristine strontium indium niobate, the bangap energy is related to the energy difference between In 5s and O 2p states. Taking into account that the substituted Pb^{IV} and Sn^{IV} ions are more electronegative than In^{III} ion [18], the Pb 6s and Sn 5s states are expected to have lower energy than In 5s state, leading to the narrowing of bandgap energy. However, even after the B-site substitution, the bandgap energy of the Sr-based compounds is still too high to absorb visible light energy. In comparison with the Sr-based compounds, the Ba-based ones have comparatively lower E_g values, as listed in Table 1. In particular, $Ba(In_{1/3}Nb_{1/3}Pb_{1/3})O_3$ shows a visible light harvesting ability with a very narrow bandgap energy of ~1.5 eV. Taking into account a pseudo-linear correlation between electronegativity and bandgap energy for the Ba-based compounds [10], such a narrow bandgap energy of $Ba(In_{1/3}Nb_{1/3}Pb_{1/3})O_3$ is surely due to the high electronegativity of tetravalent lead substitutent ion. From the present experimental findings, it becomes clear that a larger alkaline earth metal ion in A-site is more beneficial in decreasing the bandgap energy. Such an inverse proportion between radius of A-site cation and bandgap energy was further supported from the previous reports on $AIn_{0.5}Nb_{0.5}O_3$ (A = Ca, Sr and Ba) system [8a]. Kudo and co-workers also reported a similar relationship in $ATaO_3$ (A = Li, Na and K) system, but they interpreted this phenomenon in terms of the bending of Ta–O–Ta bonds, rather than the steric effect of A-site cation [11]. However, the cubic symmetry of all the materials presented here allows us to rule out the possible influence of B–O–B angle bending on the bandgap energy. In this regard, it is not necessary to consider any other possible structural effects frequently discussed such as bonding angle bending (by distortion) or lifting orbital degeneracy (by lowering symmetry), which provides the present work with a great originality. Considering the fact that the alkaline earth metal ion in this dodecahedral site with extended metal–oxygen distances does not form strong covalent bond with adjacent oxygens, this A–O bond is expected not to directly affect the band structure near Fermi energy of the perovskite-structured compound. Instead, the observed dependence of E_g on alkaline earth metal ions could be understood in terms of accompanying structural variations (i.e. a steric effect); the bigger size of Ba ion leads to the expansion of unit cell volume and hence the elongation and weakening of B–O bonds. Such a weakening of bond covalency leads to the reduced energy splitting between VB with O 2p character and CB with metal nd/($n+1$)s character, which correspond to bonding and antibonding orbitals from the viewpoint of molecular orbital approach for the BO_6 unit, as illustrated in Fig. 5. In addition to such a steric effect of the A-site cation, there is an "inductive effect" of this cation on the bandgap energy of perovskite-structured metal oxides [19]. That is, more electronegative A-site cation would decrease the electron density of adjacent B–O bonds, leading to the weakening of these bonds and the decrease of bandgap separation. It does not match with the trends in bandgap energy between

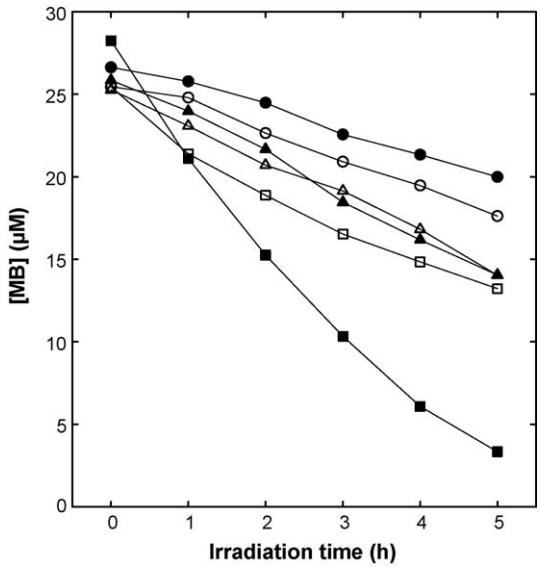

Fig. 6. Variation of MB concentration upon photoreaction with UV–vis radiations ($\lambda > 300$ nm) for $Sr(In_{1/2}Nb_{1/2})O_3$ (open circles), $Sr(In_{1/3}Nb_{1/3}Sn_{1/3})O_3$ (open triangles), $Sr(In_{1/3}Nb_{1/3}Pb_{1/3})O_3$ (open squares), $Ba(In_{1/2}Nb_{1/2})O_3$ (close circles), $Ba(In_{1/3}Nb_{1/3}Sn_{1/3})O_3$ (close triangles) and $Ba(In_{1/3}Nb_{1/3}Pb_{1/3})O_3$ (close squares).

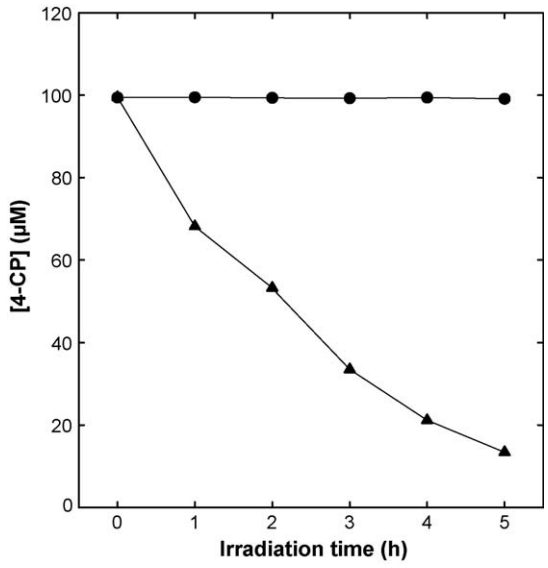

Fig. 7. Variation of 4-CP concentration upon photoreaction with visible radiations ($\lambda > 420$ nm) for $Sr(In_{1/3}Nb_{1/3}Pb_{1/3})O_3$ (circles) and $Ba(In_{1/3}Nb_{1/3}Pb_{1/3})O_3$ (triangles).

Sr- and Ba-based compounds (Table 1), which clearly demonstrates that the steric effect prevails on the inductive one in the present compounds. It is worthwhile to note here that the effect of A-site cation on the bandgap energy is more prominent for the Pb-substituted compounds than for the pristine $A(In_{1/2}Nb_{1/2})O_3$ ones. Such difference can be explained from the inductive effect; the former compounds have much stronger B–O bonds in average than the competing A–O ones, leading to the negligible inductive effect of the A-site cation on the B–O bonds. On the contrary, the B–O bond in the pristine compounds is relatively weak and hence the electronegative Sr cation can deprive of the electron density from the B–O bonds more effectively. Such a notable inductive effect in the pristine compound partially cancels out the steric effect, leading to the less prominent variation of bandgap energy upon the substitution of the A-site cation.

3.4. Characterization of photocatalytic activity

We have evaluated the photocatalytic activities of the present compounds by measuring the photodegradation of MB and 4-CP under UV–vis and visible light. In comparison with the pristine $A(In_{1/2}Nb_{1/2})O_3$, the lead-substituted $A(In_{1/3}Nb_{1/3}Pb_{1/3})O_3$ compounds result in more effective decomposition of MB under UV–vis ($\lambda > 300$ nm) radiations, see Fig. 6. Such an improvement of photocatalytic activity after the Pb substitution can be understood as a result of bandgap narrowing, leading to an additional participation of visible photonic energy in the photodegradation reaction. It is therefore quite convincing that a substitution of highly electronegative ions is very effective in improving the photocatalytic activity of semiconductors. On the other hand, we have used 4-CP as a substrate for studying the photocatalytic behavior under visible light irradiation, since the adsorption and self-sensitization of MB dye on the photocatalysts prevents from monitoring the effect of bandgap modification on visible light active photocatalysis. As can be seen clearly from Fig. 7, the $Ba(In_{1/3}Nb_{1/3}Pb_{1/3})O_3$ compound induces an effective degradation of 4-CP under visible light radiation ($\lambda > 420$ nm) whereas there is no significant change in 4-CP concentration induced with $Sr(In_{1/3}Nb_{1/3}Pb_{1/3})O_3$. Visible light driven photodegration of 4-CP by $Ba(In_{1/3}Nb_{1/3}Pb_{1/3})O_3$ was cross-confirmed by the detection of chloride ions evolved [10]. The dissimilar catalytic activites of Sr- and Ba-based compounds are in good agreement with the corresponding UV–vis results. In order to further optimize the visible light driven photocatalytic activity of $Ba(In_{0.5-x/2}Nb_{0.5-x/2}Pb_x)O_3$, we have tried to modify its bandgap energy by changing the Pb contents (x). But, the compound with higher Pb content of >0.4 could not be obtained as a pure phase, which would be due to the highly volatile nature of Pb ions. As a result of an imperfect substitution of lead ions, no prominent red shift of bandgap occurs with these compounds, compared to pure $Ba(In_{1/3}Nb_{1/3}Pb_{1/3})O_3$ compound. However, we were able to identify the increased bandgap energy of 2.0 eV with the low Pb content ($x = 0.2$). From the present experimental findings, we could conclude that the A-site cation also affects prominently the photocatalytic activity of the perovskite-type semiconductors.

4. Conclusions

In this study, we have shown that the cation substitution into the A- as well as B-sites of perovskite-structured semiconductor affects significantly its band structure and photocatalytic activity. While the substitution into the octahedral B-site leads to a direct change of CB position with metal nd/(n + 1)s character, the A-site substitution alters the bandgap energy through the variation of metal–oxygen bond strength induced by the change of unit cell volume. Based on the present results, we are able to establish two synthetic strategies for providing UV-active metal

oxide semiconductor with a visible light harvesting ability: (1) an incorporation of highly electronegative ions into the metal sites covalently bonded with oxygen ligands like octahedral B-site of perovskite structure and (2) a substitution of larger ions into space filling sites with ionic bonding character like the dodecahedral A-site of the perovskite structure. Based on these strategies, we are currently trying to prepare new efficient metal oxide photocatalysts by incorporating highly electronegative cations into the octahedral sites of Ba/Cs/Rb-based metal oxide semiconductors.

Acknowledgments

This work was supported by grant no. R08-2003-000-10409-0 from the Basic Research Program of the Korea Science & Engineering Foundation and partly by the SRC/ERC program of MOST/KOSEF (grant: R11-2005-008-03002-0). The experiments at Pohang Light Source (PLS) were supported in part by MOST and POSTECH.

References

[1] K. Honda, A. Fujishima, Nature 238 (1972) 37.
[2] (a) M.R. Hoffmann, S.T. Martin, W. Choi, D.W. Bahnemann, Chem. Rev. 95 (1995) 69;
(b) A. Mills, S.L. Hunte, J. Photochem. Photobiol. A 108 (1997) 1.
[3] (a) N. Vlachopoulos, P. Liska, J. Augustynski, M. Grätzel, J. Am. Chem. Soc. 110 (1988) 1216;
(b) E. Bae, W. Choi, J. Park, H.S. Shin, S.B. Kim, J.S. Lee, J. Phys. Chem. B 108 (2004) 14093.
[4] A. Schlafani, M.N. Mozzanega, P. Pichat, J. Photochem. Photobiol. A 59 (1991) 181.
[5] (a) T. Sato, Y. Yamamoto, Y. Fujishiro, S. Uchida, J. Chem. Soc., Faraday Trans. 92 (1996) 5089;
(b) J.H. Choy, H.C. Lee, H. Jung, S.J. Hwang, J. Mater. Chem. 11 (2001) 2232.
[6] (a) W. Choi, A. Termin, M.R. Hoffmann, J. Phys. Chem. 98 (1994) 13669;
(b) Z. Zou, J. Ye, K. Sayama, H. Arakawa, Nature 414 (2001) 625.
[7] R. Asahi, T. Morikawa, T. Ohwaki, K. Aoki, Y. Taga, Science 293 (2001) 269.
[8] (a) J. Yin, Z. Zou, J. Ye, J. Phys. Chem. B 107 (2003) 61;
(b) J. Tang, Z. Zou, J. Ye, Chem. Mater. 16 (2004) 1644.
[9] J. Yin, Z. Zou, J. Ye, J. Phys. Chem. B 107 (2003) 4936.
[10] S.G. Hur, T.W. Kim, S.J. Hwang, H. Park, W. Choi, S.J. Kim, J.H. Choy, J. Phys. Chem. B 109 (2005) 15001.
[11] (a) H. Kato, A. Kudo, J. Phys. Chem. B 105 (2001) 4285;
(b) A. Kudo, Catal. Surf. Asia 7 (2003) 31.
[12] G.A. Marking, J.A. Hanko, M.G. Kanatzidis, Chem. Mater. 10 (1998) 1191.
[13] J.H. Choy, S.J. Hwang, N.G. Park, J. Am. Chem. Soc. 119 (1997) 1624.
[14] R.D. Shannon, Acta Cryst. A 32 (1976) 751.
[15] B.K. Teo, EXAFS: Basic Principles and Data Analysis, Springer-Verlag, Berlin, 1986.
[16] K.J. Rao, J. Wong, J. Chem. Phys. 81 (1984) 4832–4843.
[17] (a) L. Pauling, The Nature of the Chemical Bond, third ed., Cornell University, Ithaca, New York, 1960, p. 93;
(b) A.L. Allred, J. Inorg. Nucl. Chem. 17 (1961) 215.
[18] Electronegativity of the component metal, cations from ref. [17]: $\chi_{\text{Pauling}}(\text{InIII}) = 1.78$, $\chi_{\text{Pauling}}(\text{NbV}) = 1.6$, $\chi_{\text{Pauling}}(\text{SnIV}) = 1.96$, $\chi_{\text{Pauling}}(\text{PbIV}) = 2.33$.
[19] (a) J. Etourneau, J. Portier, J. Alloys Compd. 188 (1992) 1;
(b) A. Yamamoto, N.R. Khasanova, F. Izumi, X.-J. Wu, T. Kamiyama, S. Torii, S. Tajima, Chem. Mater. 11 (1999) 747.